

# Graphene-nanoparticle incorporated responsivity tuning of p-CuO/n-Si-based heterojunction photodetectors

JENIFAR SULTANA<sup>1</sup>, ANANNYA BHATTACHARYA<sup>2</sup>, ANUPAM KARMAKAR<sup>2</sup>,  
GOUTAM K DALAPATI<sup>3</sup> and SANATAN CHATTOPADHYAY<sup>2,\*</sup>

<sup>1</sup>Centre for Research in Nanoscience and Nanotechnology (CRNN), Kolkata 700098, India

<sup>2</sup>Department of Electronic Science, University of Calcutta, Kolkata 700009, India

<sup>3</sup>Institute of Materials Research and Engineering, A\*STAR (Agency for Science, Technology and Research),

2 Fusionopolis Way; Innovis #08-03, Singapore 138634, Singapore

\*Author for correspondence (scele@caluniv.ac.in)

MS received 30 October 2018; accepted 4 March 2019; published online 14 June 2019

**Abstract.** The current work focusses on investigating the appropriate wt% of graphene-nanoparticles to be incorporated into the CuO film as a dopant for enhancing its optoelectronic properties. CuO and graphene-nanoparticle-incorporated CuO films (CG) are grown by employing a chemical bath deposition (CBD) method. Graphene-nanoparticles have been incorporated at different wt% (1, 5 and 10%) with respect to the metal salt (CuCl<sub>2</sub>·2H<sub>2</sub>O), and a comparative study has been performed on the systematic change of the film morphology, chemical composition, oxidation states, crystallite structures and photo-sensing effects. It has been found that the morphology and the structural properties of CBD grown CuO films have been tuned by the incorporation of graphene-nanoparticles. The results show a significant enhancement in the optoelectronic properties of CG1 (1%) and CG5 (5%) films. The optical properties of the as-grown films have been observed to be modified by graphene-nanoparticle incorporation. Moreover, the electronic and optoelectronic characteristics of the fabricated p-CuO/n-Si heterojunctions have also been investigated. The enhancement of the optoelectronic properties of the CG5 sample as compared to other grown films in the present study suggests that the responsivity and photodetecting properties of the CBD grown CuO films can be improved by graphene-nanoparticle incorporation.

**Keywords.** Graphene-nanoparticle; CuO; CBD; responsivity; photodetector.

## 1. Introduction

Photodetectors (PDs) based on semiconductor nanostructures have drawn significant research interest in recent years not only as a single-function device in detecting optical signals, but also as an elementary component for nano-optoelectronic systems [1–3]. The basic requirement which an ideal PD must satisfy is high speed responsivity. Additionally, PDs, based on the photovoltaic effect are competent to operate without external bias. This type of self-powered PD has become highly desirable in recent years to meet the global energy crisis [4]. The major commercial materials used for PDs, such as GaN, Si and InGaAs are operational only in UV, visible and near-infrared sub-bands, respectively. Moreover, it is costly and complicated to fabricate highly crystalline junctions [5]. Therefore, it would be greatly beneficial to investigate novel junction architectures of PDs with a multispectral response and low cost to further improve the performance [6].

One of the possible solutions to the above problem is to propose a novel heterojunction structure of the photodetector with suitable materials having excellent optoelectronic transfer efficiency [6,7]. In this context, metal–oxide thin films,

such as copper oxides (CuO) have drawn significant research interest owing to their multifaceted applications in the areas of electronics, optoelectronics, energy scavenging and catalysis [8–11]. The relatively smaller band gap of CuO makes it a potentially superior material for photodetection and optical switching applications in the visible or near-infrared region [12]. In this context, it finds a wide range of applications in the domain of energy harvesting and storage [13], photoelectrochemical cells [14], photocatalysts and photovoltaic devices [15,16].

CuO thin films can be easily grown by different techniques including the reactive sputtering [17], chemical vapour deposition [18], chemical conversion [19], vapour liquid solid [20], thermal oxidization [21], rapid precipitation, spin coating [22], solid state reaction [23], sol–gel techniques [24] and hydrothermal method [25]. Also, the performance of such films developed by each of these individual techniques has been reported [13,24]. Under such circumstances, chemical bath deposition (CBD) is a growth process that has drawn considerable attention due to its simplicity, cost-effectiveness, reproducibility and ability of large area scaling for commercial production [3,25,26]. The deposition rate and hence, the

thickness of the deposited film can be precisely controlled by varying pH, temperature and concentration of the solution.

Graphene-nanoparticles exhibit unique structural geometry and fascinating physical properties and hence, have great prospects in applied electronics [27–30]. Also, they are extensively used in a composite material to improve the electrical and mechanical properties of its host matrix. Graphene-nanoparticles when merged with the semiconductor system, enhance the optoelectronic properties of the system owing to their exceptional electron transport properties [27]. Being a good electron acceptor, they enhance the charge carrier separation and hence, the photocatalytic activity of the host semiconductor system. Reports are also available to indicate that the electrical and optical properties of the CuO-based devices can be significantly improved by graphene-nanoparticle addition [30]. Thus, investigation of the appropriate optimized doping percentage of graphene-nanoparticles in CuO films is immensely crucial for their suitable use in the areas of nano-electronics, optoelectronics and photodetection.

In the current study, graphene-nanoparticles have been used in different ratios to dope CuO and thus, the optoelectronic properties of the CuO film have been tuned with graphene-nanoparticles. Both the CuO and graphene-nanoparticle incorporated CuO film have been grown by the CBD technique. The changes in the surface morphology, crystallite quality and the chemical states of the as-deposited CuO films have been studied with the addition of graphene-nanoparticles. Field emission scanning electron microscopy (FESEM), energy dispersive X-ray (EDX) spectroscopy, X-ray diffraction (XRD) and X-ray photoelectron spectroscopy (XPS) measurements have been employed for the structural and elemental characterization of the grown CuO films. The optical and optoelectronic properties of the grown films have been investigated by spectroscopic ellipsometric (SE) and responsivity measurements. Improvement in the optoelectronic properties of the CG5 film proves that graphene-nanoparticles to be a potential material as a dopant of CuO for optoelectronic applications.

## 2. Experimental

The thin film of CuO has been grown on an n-silicon substrate by the CBD technique. For the growth of the CuO thin film, 1.705 g  $\text{CuCl}_2 \cdot 2\text{H}_2\text{O}$  was dissolved in 100 ml of deionized (DI) water to make 0.1 M solution under constant stirring. To incorporate graphene-nanoparticles into the CuO film, initially graphene oxide was indigenously synthesized by modified Hummer's method and then, graphene nanoparticles were obtained by a thermal reduction method. The particle size has been obtained to be in the order of 80–100 nm. These graphene nanoparticles were further used to grow the CG samples. Graphene-nanoparticles, in three different wt% of 0.1 M  $\text{CuCl}_2 \cdot 2\text{H}_2\text{O}$  (1, 5 and 10%) i.e., 0.0175, 0.085 and

0.1705 g, were added to the above made solution. The solution was sonicated by using a sonicator (LMUC series) for 5 min, followed by continuous stirring before growth. Initially, the Si wafers were cleaned by standard RCA-I and RCA-II processing followed by native oxide removal. The cleaned wafers were then dipped vertically into the prepared solutions under constant stirring and heating. When the bath temperature rises to 60°C, 5 ml of ammonia solution ( $\text{NH}_3 + \text{H}_2\text{O}$ ) was added drop-by-drop to the reaction mixture and the solution was heated at 85°C with constant stirring and the deposition has been performed for 25 min. Thus, four samples, with a percentage of graphene-nanoparticles as 0, 1, 5 and 10%, were prepared and were named as CuO, CG1, CG5 and CG10. Post-deposition cleaning was performed in running DI water to remove the residual solutes and impurities and further dried by blowing nitrogen ( $\text{N}_2$ ) gas. The as-deposited CuO and CG films were compared in terms of their structural, optical and electrical properties. For device fabrication, Ag dots with a diameter of 0.5 mm were deposited on the as-deposited films to form p-CuO/n-Si diodes. The surface morphology of the grown samples has been investigated, by using FESEM (JEOL FESEM JSM 6700F). Elemental and compositional analyses are performed by EDX (JEOL JSM 6700F) analysis. The structural and crystallographic orientations are conducted by employing the XRD. The chemical nature and oxidation states of copper on the surface of the samples were examined by XPS analysis. The XPS data are deconvoluted using Peak Fit software (version 4.12). SE was used to analyse the absorption coefficient ( $\alpha$ ) and optical band gap ( $E_g$ ) of all the as-deposited samples on the Si substrate. The current–voltage ( $I-V$ ) and photoresponsivity measurements of the p-CuO/n-Si heterojunctions were performed by using a Keithley parameter analyser.

## 3. Results and discussion

Figure 1a–h shows the FESEM micrographs of the as-deposited CuO, CG1, CG5 and CG10 samples, respectively, in both low (1  $\mu\text{m}$ ) and high (100 nm) magnification scales.

The CuO sample shows a nonuniform film like morphology with no well-defined grain boundaries, however, graphene-nanoparticle incorporation shows a change in the morphology to a nanofibre and nanoflake type as depicted in figure 1c–h. Also, with an increase in the percentage of graphene-nanoparticles from 1 to 5%, the density of the nanofibres increases as shown in figure 1c–f. As the percentage of graphene-nanoparticles increases to 10%, the morphology changes to nanoflakes as evident from figure 1g and h.

The comparative EDX spectra of the as-deposited CuO, CG1, CG5 and CG10 samples are measured by employing the JEOL-JSM 7600F FESEM system and are shown in figure 2a–d, respectively. The corresponding surface morphology is also shown along with the EDX spectra. All the samples show the presence of copper (Cu) and oxygen (O).

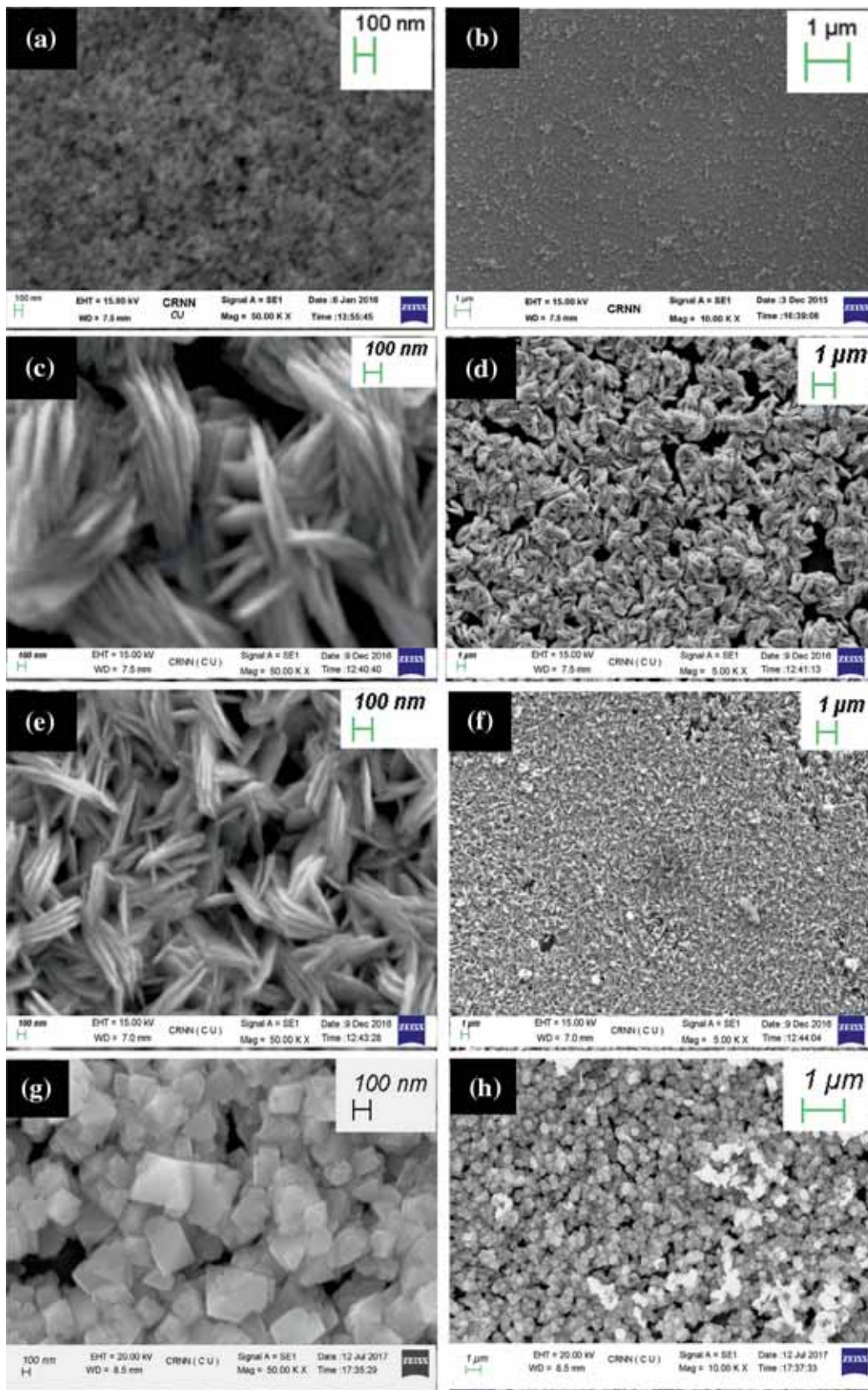


**Figure 1.** FESEM images of the CBD grown CuO and graphene incorporated CuO thin films at low (1  $\mu\text{m}$ ) and high (100 nm) magnification scales: (a, b) CuO, (c, d) CG1, (e, f) CG5 and (g, h) CG10 samples.

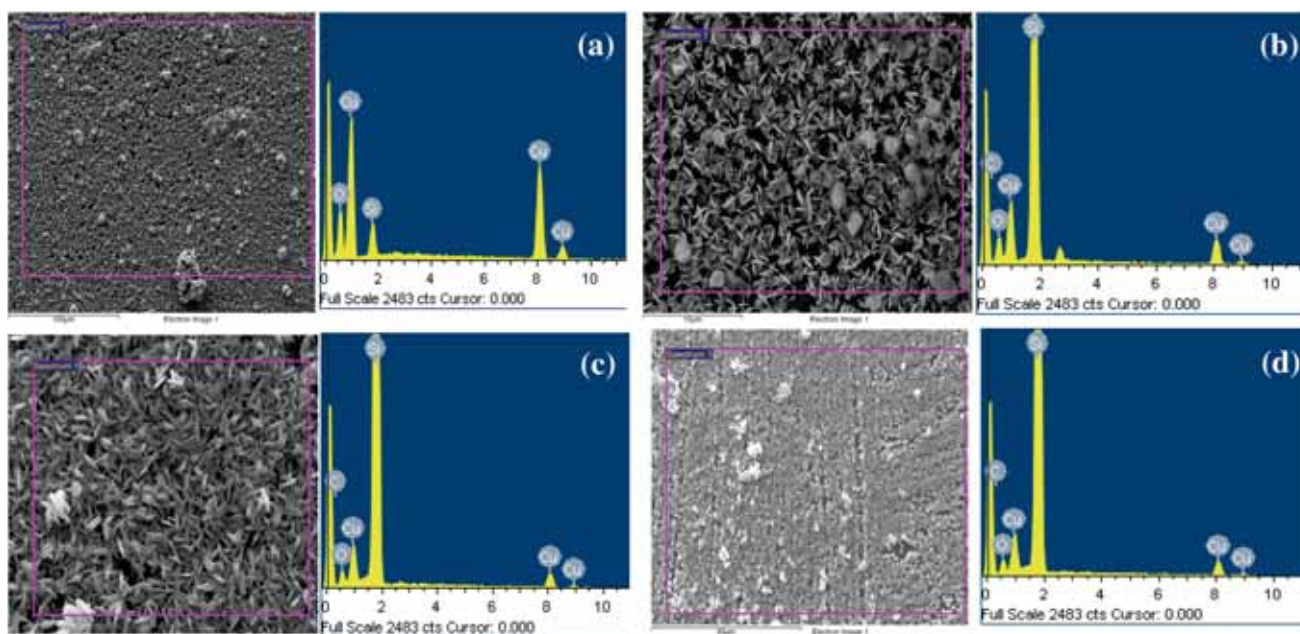


**Figure 2.** Comparative plots of EDX spectra for the as-deposited (a) CuO, (b) CG1, (c) CG5 and (d) CG10 samples.

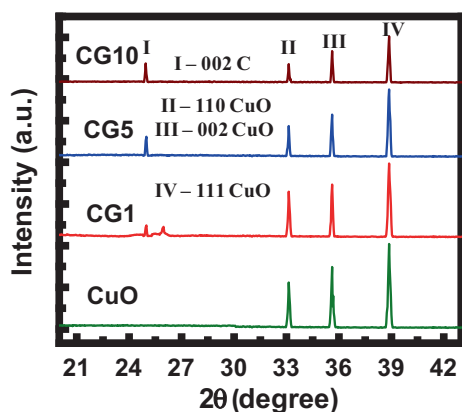


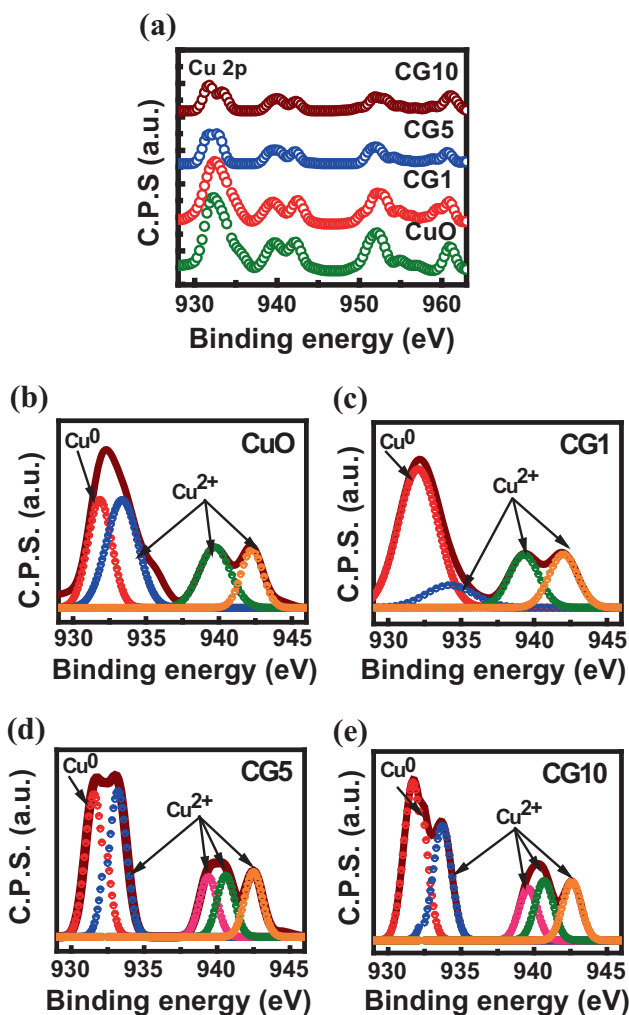
**Figure 3.** Comparative plots of XRD patterns for the as-deposited CuO, CG1, CG5 and CG10 samples where peak I corresponds to the [002] plane of graphite and II, III and IV correspond to [110], [002] and [111] planes of CuO, respectively.

The crystallographic and structural orientations of the grown CuO and CG films have been investigated by XRD measurements and the relevant spectra are shown in figure 3. All the samples exhibit diffraction peaks corresponding to monoclinic CuO, which is verified by JCPDS card no. 80-1917 [8]. The peaks II, III and IV correspond to 110, 002 and 111 planes of CuO. It is also apparent from the XRD spectra that the CG1, CG5 and CG10 samples also exhibit a comparatively low intensity peak at  $\sim 25^\circ$  (numbered I), which is indexed to be the (002) plane of the hexagonal graphite structure suggesting that the graphene-nanoparticles are incorporated into the CG samples [31,32]. Moreover, the

basal spacing calculated from the XRD data by Bragg's law has been found to be 0.343, 0.346 and 0.347 nm for CG1, CG5 and CG10 samples, respectively. According to Saito *et al* [33], the basal distance for pure graphene is around 0.34 nm. Thus, the presence of graphene in the CG samples can be confirmed from the basal spacing data as reported in the literature [34]. The low intensity could be attributed to the relatively low amount and low diffraction intensity of graphene-nanoparticles as compared to CuO. Also, the peak corresponding to graphite seems to increase with the percentage of graphene-nanoparticles from 1 to 10%. As the diffraction patterns of the CG films are a superposition of both CuO and graphite, thus, clearly confirming that the graphene-nanoparticles have been effectively incorporated into the CuO films.

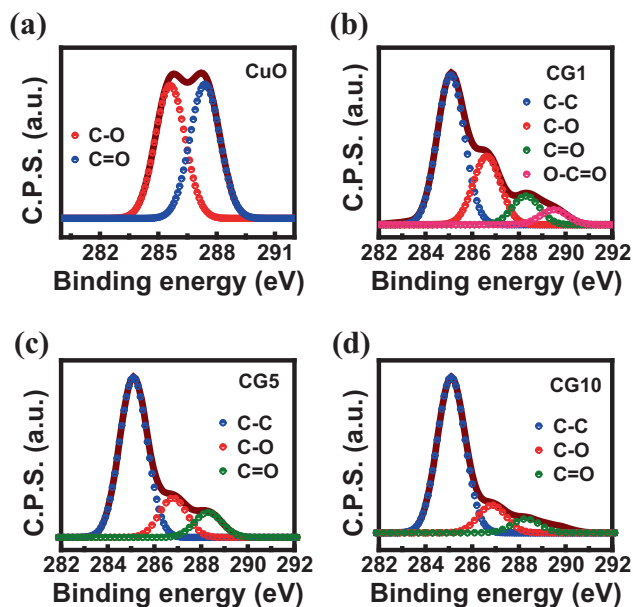
To investigate the elemental composition and the chemical states of the grown samples, XPS measurements are conducted in the VG ESCALAB 220i-XL XPS system with a monochromatic AlK $\alpha$  source (1486.6 eV electron energy analyser using AlK $\alpha$  photons) in an ultrahigh vacuum chamber. The XPS spectra are analysed using the Peak-Fit software (Peak-Fit version 4.12) and the detailed results are shown in figures 4a–e, 5a–d and 6a–d, respectively. The relevant fitting parameters used for peak deconvolution are summarized in table 1.

Figure 4a shows the high resolution Cu 2p doublet XPS spectra of the grown CuO films with different graphene-nanoparticle compositions. Also, to obtain more information about the oxidation states of Cu, the main Cu 2p $_{3/2}$  photoelectron peak along with its satellite are deconvoluted and are shown in figure 4b–e, respectively. It is worth noting that the Cu 2p XPS spectra of all the grown samples show



**Figure 4.** (a) Cu 2p XPS spectra of the as-deposited CuO and CG films and deconvoluted XPS spectra of the Cu 2p<sub>3/2</sub> main line and its corresponding satellite line of (b) CuO, (c) CG1, (d) CG5 and (e) CG10 samples.

Cu 2p<sub>3/2</sub> and 2p<sub>1/2</sub> doublet peaks along with their satellite lines, the latter being indicative of the Cu<sup>2+</sup> state. It is apparent from figure 4a that Cu 2p<sub>3/2</sub> and 2p<sub>1/2</sub> doublet peaks are observed at ~932.4 and 952.2 eV, respectively, with a spin-orbit splitting of 19.8 eV and small shoulder peaks are observed near the main peaks at ~935 and 955 eV, respectively. The main sharp Cu 2p<sub>3/2</sub> peak indicates the formation of metallic Cu (Cu<sup>0</sup>) and Cu<sup>2+</sup> phases. The main Cu 2p peaks are accompanied by satellite lines at relatively higher binding energy of ~9 eV. Such satellite lines are attributed to the characteristic features of the materials with a d<sup>9</sup> configuration at the ground state, and due to the multiplet splitting of the 2p<sup>5</sup>3d<sup>9</sup> final state band, thereby, confirming the formation of CuO [8]. This indicates that Cu<sup>0</sup>/Cu<sup>+</sup> and Cu<sup>2+</sup> phases co-exist in all the grown films with varying graphene-nanoparticle compositions. To obtain further information regarding the oxidation state of Cu, the Cu 2p<sub>3/2</sub> primary



**Figure 5.** Deconvoluted C 1s XPS spectra of: (a) CuO, (b) CG1, (c) CG5 and (d) CG10 samples.

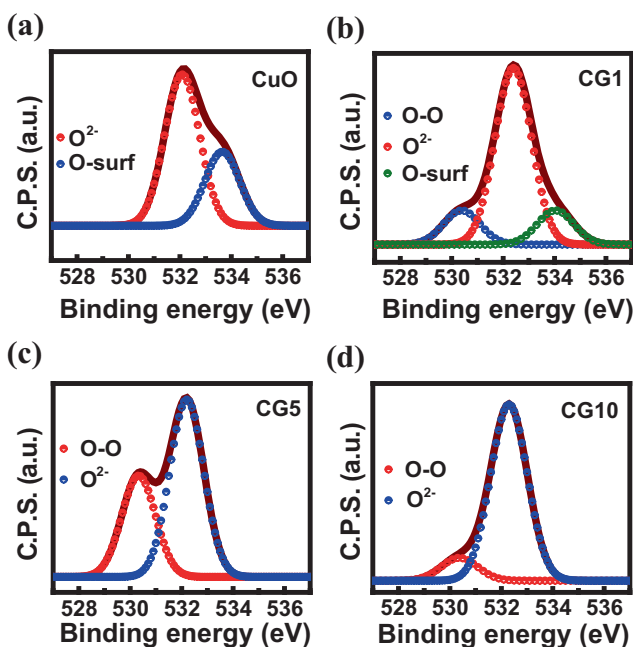


**Figure 6.** Deconvoluted O 1s XPS spectra of: (a) CuO, (b) CG1, (c) CG5 and (d) CG10 samples.

peak and its corresponding satellite peak for all the films are deconvoluted as shown in figure 4b–e, respectively. The peak fit of the main Cu 2p peak of all the samples corresponds to two peaks at ~932.2 and 933.3 eV which are indicative of metallic Cu (Cu<sup>0</sup>) and CuO (Cu<sup>2+</sup>) phases along with two shake up satellite peaks of CuO at 939.7 and 942 eV, respectively [8]. Also, it is interesting to note from figure 4 that

**Table 1.** Fitting parameter ( $r^2$  coefficient of determination) for Cu 2p, C 1s and O 1s for all the as-deposited CuO and CG samples.

Sample/phase	CuO	CG1	CG5	CG10
Cu 2p	0.965	0.964	0.984	0.978
C 1s	0.987	0.996	0.998	0.998
O 1s	0.989	0.998	0.993	0.996

the intensity of the Cu 2p peaks decreases with an increase in graphene composition which is indicative of the fact that the corresponding phases of Cu decrease, which corroborates with the XRD data.

To reveal information regarding the nature of carbon associated with the grown films, the C 1s spectrum is deconvoluted and is shown in figure 5a–d, respectively. The C 1s spectrum of the graphene-nanoparticle incorporated CuO films has a sharp peak at  $\sim 284.8$  eV along with other small peaks at higher binding energies. However, the C 1s spectrum of the pure CuO film shows a broad peak at  $\sim 286$  eV. As shown in figure 5a, the C 1s region of the pure CuO film is fitted by two sub-peaks at  $\sim 286.8$  and  $287.6$  eV corresponding to C–O and C=O groups, respectively. C 1s spectra of all the graphene-nanoparticle incorporated CuO films show a sharp peak at  $\sim 284.8$  eV corresponding to the C–C (C in graphene) group along with other small peaks as shown in figure 5b–d, respectively [31]. The CG1 sample shows four peaks  $\sim 284.8$ ,  $286.8$ ,  $287.6$  and  $288.7$  eV corresponding to C–C, C–O, C=O and O–C=O groups, respectively. Also, CG5 and CG10 samples show three peaks  $\sim 284.8$ ,  $286.8$  and  $287.6$  eV corresponding to C–C, C–O and C=O groups, respectively [31]. Again, it is worth to note from figure 5a–d that with an increase in the percentage of graphene, the main carbon peak corresponding to graphene at  $284.8$  eV became predominant, while the others markedly decreased, indicating the removal of oxygen-containing functional groups.

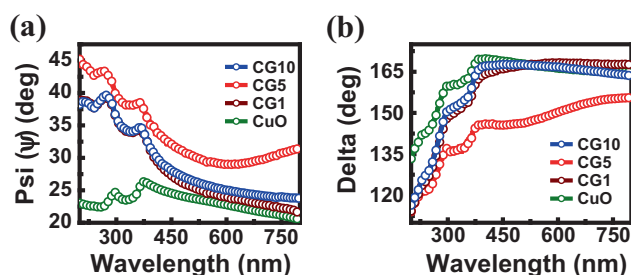
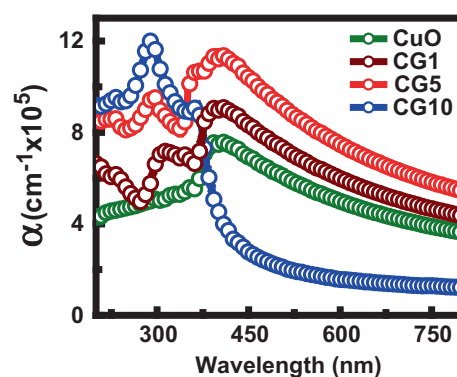
The deconvoluted O 1s spectra of the as-deposited CuO and CG samples are shown in figure 6a–d, respectively. It is evident from figure 6a–d that the main peak at  $\sim 532.3$  eV for all the samples is originated from the lattice oxygen  $O^{2-}$ . The peak at  $530.1$  eV is attributed to the O–O bond [35]. Furthermore, the broad peak at  $534.3$  eV is attributed to the adsorbed oxygen in the surface of the film [8].

Moreover, the peak area ratios of O 1s peaks have also been determined and tabulated in table 2. It is evident from the table that the peak area of the main peak ( $\sim 532.3$  eV) originating from lattice oxygen ( $O^{2-}$ ) increases with an increase in graphene-nanoparticle concentration. This is attributed to the fact that the contribution from the surface adsorbed oxygen and O–O bond decreases with an increase in graphene-nanoparticle concentration as these bonds are replaced with C–C bonds of graphene-nanoparticles.

To investigate the effect of graphene-nanoparticles on the optical properties of the CuO film, SE measurements have

**Table 2.** Peak areas of the deconvoluted O 1s peaks of the as-deposited CuO and CG samples.

Sample/peak area	$O^{2-}$	O–O	Adsorbed oxygen
CuO	65.52	—	34.48
CG1	72.21	13.73	14.06
CG5	75.56	24.44	—
CG10	89.45	10.55	—

**Figure 7.** Plot of ellipsometric parameters: (a) psi ( $\Psi$ ) and (b) delta ( $\Delta$ ) in the wavelength range of 250–800 nm for the grown samples.**Figure 8.** Plot of the extracted absorption coefficient with wavelength for the grown samples.

been performed in the spectral range of 250–800 nm. The respective  $\Psi$  (the amplitude ratio between reflected and polarized components ( $p$ )) and  $\Delta$  (phase difference between the reflected and polarized components) have been measured for the angle of incidence of  $60^\circ$  and the comparative plots are shown in figure 7. The measured  $\Psi$  and  $\Delta$  are utilized to determine the extinction coefficient and hence, the absorption coefficient of the grown CuO and CG samples. The variation of absorption coefficients of the as-deposited films with wavelength is shown in figure 8.

Generally, two kinds of characteristic features have been reported in the spectra of graphene. One is at  $\sim 310$  nm, corresponding to an  $n-\pi^*$  plasmon peak. Another characteristic peak appears at  $\sim 230$  nm which corresponds to a  $\pi-\pi^*$  plasmon peak [36]. It is apparent from the plot that

the CuO film has a characteristic peak at ~420 nm. However, with the addition of graphene-nanoparticles, the absorption coefficient increases in the considered wavelength range, except for the CG10 sample, along with an extra peak at ~310 nm which is considered to be the contribution of graphene-nanoparticles corresponding to the  $n-\pi^*$  plasmon. As the percentage of graphene-nanoparticles increases, the absorption peak intensity at ~310 nm also increases. With an increase in graphene-nanoparticles, the enhancement in absorbance is attributed to the increase of surface electric charge of the oxides and the modification of the fundamental process of electron-hole pair formation during irradiation [30]. For the CG10 sample, the contribution from graphene-nanoparticles is the highest and CuO absorption is the lowest and hence, the peak at ~310 nm is maximum for the CG10 sample.

The electrical characterization of the grown heterojunctions has been performed by measuring the current-voltage ( $I-V$ ) characteristics under both dark and illuminated conditions by varying the light intensity (1–10  $\text{mW cm}^{-2}$ ) and also by using light of different wavelengths ranging from 300 to 1000 nm.

To investigate the photodetecting performance of the fabricated photodetectors, the photoresponsivity has been measured, which indicates how efficiently a detector responds to optical signals. It is generally expressed by the equation  $R = (I_{\text{photon}} - I_{\text{dark}})/P_{\text{in}}$ , where  $I_{\text{photon}}$ ,  $I_{\text{dark}}$  and  $P_{\text{in}}$  are the photocurrent, dark current and illumination power on the active area of the photodetector, respectively [7]. To demonstrate the effectiveness of graphene-nanoparticles on CuO-based photodetectors, the photoresponsivity has been measured with respect to the applied reverse bias voltage and graphene-nanoparticle percentage and is shown in figure 9a–c. It is apparent from the figures that the photoresponsivity is maximum for the CG5 sample and it also increases with applied reverse bias. The increase of responsivity for the CG5 sample may be attributed to the improved conductivity provided by graphene-nanoparticle incorporation, which acts as a conductive electron transport path [30]. Moreover, the change in the morphology to nanostructures as depicted from SEM images may also contribute to the improved absorption and hence photoresponsivity.

However, for the CG10 sample, the decrease in responsivity as compared to CG5 may be attributed to the increase in the absorption of graphene-nanoparticles (in UV range) as compared to CuO (in visible range). Thus, the overall responsivity under white light illumination decreases. This result also corroborates well with the optical and XPS data.

The responsivity of the photodetectors has also been plotted with varying light intensities and is shown in figure 10a–d. It is apparent from the plot that responsivity increases with an increase in the light intensity for all the photodetectors. To demonstrate the effectiveness of graphene-nanoparticles in improving the photovoltaic performance of CuO-based photodetectors, the photoresponsivity at 0 V bias has been measured under illumination of different wavelength lights

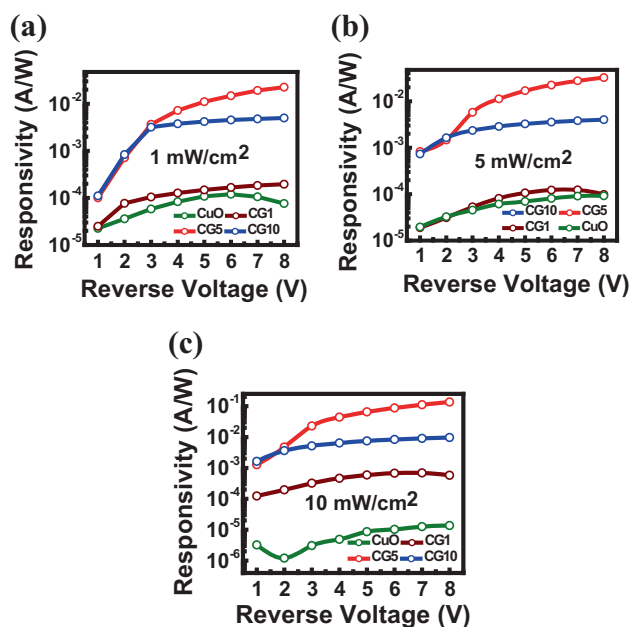


**Figure 9.** Variations in the responsivity of the photodetectors with graphene concentration as a function of reverse bias voltage under different light illuminations: (a) 1, (b) 5 and (c) 10  $\text{mW cm}^{-2}$ .

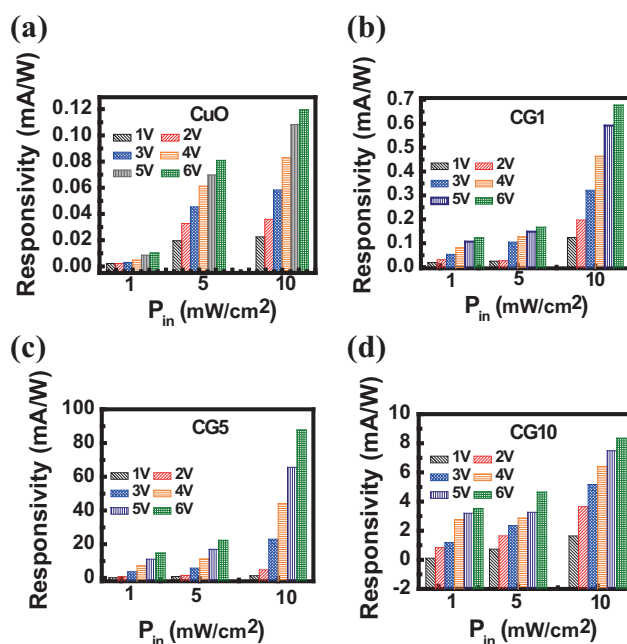


**Figure 10.** Variations in the responsivity with light intensity of the photodetectors based on (a) CuO, (b) CG1, (c) CG5 and (d) CG10 samples at different reverse biases.

(300–1000 nm) and is shown in figure 11a. Also, the corresponding photovoltage generated is shown in figure 11b.

The variation of responsivity with wavelength at different reverse bias voltages of the grown samples is also shown in figure 12a–d. It is clear from the plots that both the

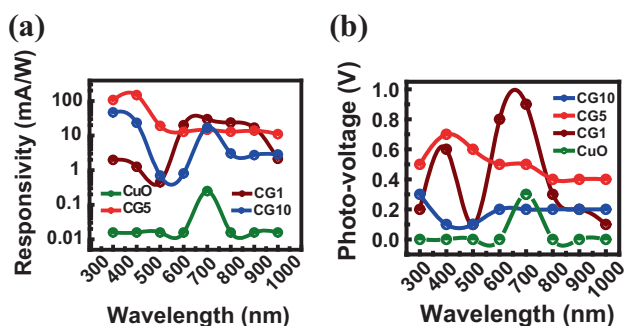


**Figure 11.** (a) Responsivity at 0 V bias and (b) photovoltage of the fabricated heterojunctions under light illumination of different wavelengths (300–1000 nm).

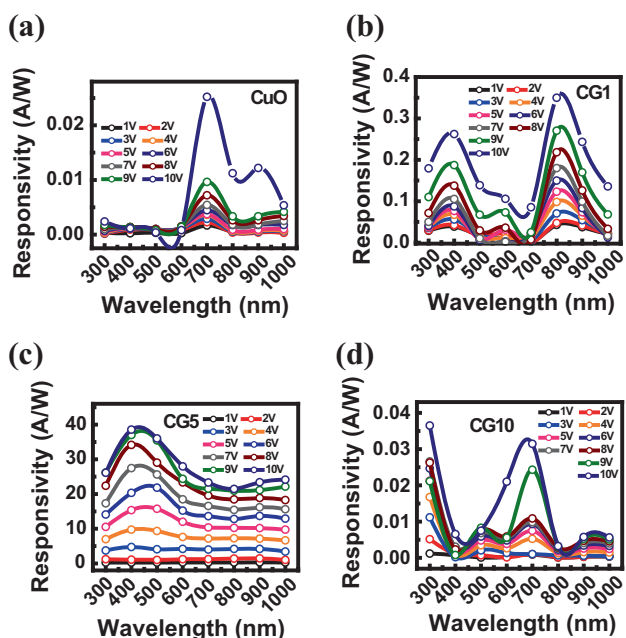


**Figure 12.** Variations in responsivity with wavelength (300–1000 nm) at different reverse bias voltages for (a) CuO, (b) CG1, (c) CG5 and (d) CG10 samples.

responsivity and photovoltage at 0 V bias have been increased by the addition of graphene-nanoparticles as compared to CuO, which is attributed to the enhanced electron collection efficiency by graphene-nanoparticles. The migration of electrons from the CuO film to the graphene-nanoparticle results in a separation of electrons and holes. This effectively reduces the recombination rate of the photogenerated charge carriers and enhances the electron collection efficiency, leading to an improvement in responsivity and photovoltage. However, the CG10 sample shows lower responsivity and photovoltage at 300 nm as compared to CG5. This can be explained by the fact that for the CG10 sample, the  $\pi$ - $\pi^*$  plasmon peak is more dominating than the  $n$ - $\pi^*$  plasmon peak. The  $\pi$ - $\pi^*$  plasmon peak depends on two kinds of conjugative effects: one is related to nanometre-scale  $sp^2$

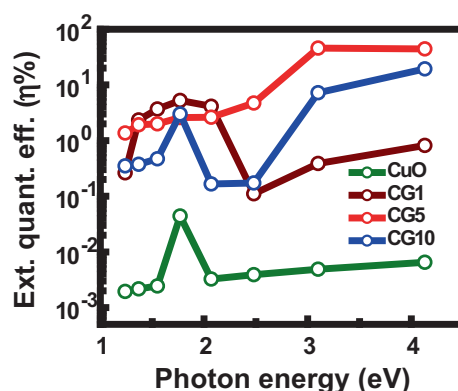


**Figure 13.** Variations of external quantum efficiency at 0 V bias with photon energy of the fabricated photodetectors.

clusters and the other arises from linking chromophore units, such as C=C, C=O and C-O bonds [36]. XPS data reveal that there is an increase in the deconvoluted peaks corresponding to C=C at 284.8 eV, while the others (C=O and C-O) are markedly decreased, indicating the removal of oxygen-containing functional groups for the CG10 sample as compared to other graphene containing samples. Now, since  $sp^2$  nanoclusters also contain C=C bonds, so, the decrease in photoresponsivity can be attributed to an increase in C=C bonds for the CG10 samples. Based on the above facts, it is inferred that the change in the photoresponsivity observed for CG10 is caused by the conjugative effect of  $sp^2$  clusters, which influences the  $\pi$ - $\pi^*$  plasmon peak [35].

The variation of external quantum efficiency with photon energy is shown in figure 13. It is clear from the figure that the external quantum efficiency for the CG5 sample is much more enhanced as compared to other samples, mainly in the wavelength range of 300–500 nm. Also, in the visible and NIR ranges, it has improved efficiency as compared to the as-deposited CuO sample. Thus, the CG5 sample proves to be the suitable material for photodetection in the range of 300–1000 nm.

#### 4. Conclusions

CuO and graphene-nanoparticle incorporated CuO films have been grown by the CBD method. To study the effect of graphene-nanoparticles on CuO-based photodetectors, three samples have been prepared by varying the concentration of graphene-nanoparticles from 1 to 10%. The morphology, optical properties and photosensitivity of CuO films have been systematically studied with graphene-nanoparticle concentration. It has been observed that the incorporation of graphene-nanoparticles has a significant impact on the CuO film morphology and its optoelectronic property. The crystalline nature and compositional analysis of the film are

determined by XRD, EDX and XPS studies and the optical properties are investigated by SE analysis. Five percent graphene–nanoparticles addition to the CuO film has been found to be the best for developing a p-CuO/n-Si junction for optoelectronic applications and has been observed to deliver the best optical and electrical performance compared to the other graphene nanoparticle concentrations considered in the current work. The improvement of the CG5 film-based photodetector is due to the increased conductivity of the film and suppression of charge carrier recombination.

### Acknowledgements

Miss Jenifar Sultana likes to acknowledge the Department of Science and Technology (DST), India, for providing inspire fellowship to pursue her research. We would also like to acknowledge the DST Purse program and Center of Excellence (COE), TEQIP, for providing infrastructure and financial support to conduct this work.

### References

- [1] Kim C O, Kim S, Shin D H, Kang S S, Kim J M, Jang C W *et al* 2014 *Nat. Commun.* **5** 3249
- [2] Manders J R, Lai T H, An Y, Xu W, Lee J, Kim D Y *et al* 2014 *Adv. Funct. Mater.* **24** 7205
- [3] Wang L, Jie J, Shao Z, Zhang Q, Zhang X, Wang Y *et al* 2015 *Adv. Funct. Mater.* **25** 2910
- [4] Zhang Z, Liao Q, Yu Y, Wang X and Zhang Y 2014 *Nano Energy* **9** 237
- [5] Yuan H, Liu X, Afshinmanesh F, Li W, Xu G, Sun J *et al* 2015 *Nat. Nanotechnol.* **10** 707
- [6] Su G, Hadjiev V G, Loya P E, Zhang J, Lei S, Maharajan S *et al* 2015 *Nano Lett.* **15** 506
- [7] Zhao C, Liang Z, Su M, Liu P, Mai W and Xie W 2015 *ACS Appl. Mater. Interfaces* **7** 25981
- [8] Sultana J, Paul S, Karmakar A, Yi R, Dalapati G K and Chattopadhyay S 2017 *Appl. Surf. Sci.* **418** 380
- [9] Sultana J, Paul S, Karmakar A, Dalapati G K and Chattopadhyay S 2018 *J. Mater. Sci.: Mater. Electron.* **29** 12878
- [10] Mittiga A, Salza E, Sarto F, Tucci M and Vasanthi R 2006 *Appl. Phys. Lett.* **88** 163502
- [11] Mahalingam T, Chitra J S P, Chu J P, Moon H, Kwon H J and Kim Y D 2006 *J. Mater. Sci.: Mater. Electron.* **17** 519
- [12] Jin Z, Zhang X, Li Y, Li S and Lu G 2007 *Catal. Commun.* **8** 1267
- [13] Fu L, Gao J, Zhang T, Cao Q, Yang L C, Wu Y P *et al* 2007 *J. Power Sources* **171** 904
- [14] Nakamura Y, Zhuang H, Kishimoto A, Okada O and Yanagida H 1998 *J. Electrochem. Soc.* **145** 632
- [15] Chen J, Huang N Y, Deng S Z, She J C, Xu N S, Zhang W X *et al* 2005 *Appl. Phys. Lett.* **86** 157
- [16] Sultana J, Das A, Das A, Saha N R, Karmakar A and Chattopadhyay S 2016 *Thin Solid Films* **612** 331
- [17] Christie E A 1970 *Proceedings of International Solar Energy Society Conference*, pp 1–7
- [18] Musa A O, Akomolafe T and Carter M J 1998 *Sol. Energy Mater. Sol. Cells* **51** 305
- [19] Brookshier M A, Chusuei C C and Goodman D W 1999 *Langmuir* **15** 2043
- [20] Xu J F, Ji W, Shen Z X, Tang S H, Ye X R, Jia D Z *et al* 1999 *J. Solid State Chem.* **147** 516
- [21] Su Y K, Shen C M, Yang H T, Li L and Gao H J 2007 *Trans. Nonferr. Met. Soc. China* **17** 783
- [22] Tang X L, Ren L, Sun L N, Tian W G, Cao M H and Hu C W 2006 *Chem. Res. Chin. Univ.* **22** 547
- [23] Yuan C O, Jiang H F, Lin C and Liao S J 2007 *J. Cryst. Growth* **303** 400
- [24] Chen J T, Zhang F, Wang J, Zhang G A, Mian B B, Fan X Y *et al* 2008 *J. Alloys Compd.* **454** 268
- [25] Nair P K, Nair M T S, Garcia V M, Arenas O L, Pena Y, Castillo A *et al* 1998 *Sol. Energy Mater. Sol. Cells* **52** 313
- [26] Nair P K, Parmananda P and Nair M T S 1999 *J. Cryst. Growth* **206** 68
- [27] Lancellotti L, Polichetti T, Ricciardella F, Tari O, Gnanapragasam S, Daliento S *et al* 2012 *Thin Solid Films* **522** 390
- [28] Wu Z S, Zhou G, Yin L C, Ren Y, Li F and Cheng H M 2012 *Nano Energy* **1** 107
- [29] Tran P D, Batabyal S K, Pramana S S, Barber J, Wong L H and Loo S C J 2012 *Nanoscale* **4** 3875
- [30] Panah S M, Kakran M, Lim Y F, Chua C S, Tan H R and Dalapati G K 2016 *J. Renew. Sustain. Energy* **8** 043507
- [31] Liua X, Pana L, Zhaob Q, Lva T, Zhua G, Chena T *et al* 2012 *Chem. Eng. J.* **183** 238
- [32] Zhao B, Liu P, Zhuang H, Jiao Z, Fang T, Xu W *et al* 2013 *J. Mater. Chem. A* **1** 367
- [33] Saito R, Dresselhaus G and Dresselhaus M S 2005 *Physical properties of carbon nanotubes* (London: Imperial College Press) 2nd edn
- [34] Avila A F, Peixoto L G Z, Neto A S, Junior J and Carvalho M G R 2012 *J. Braz. Soc. Mech. Sci. Eng.* **3** 269
- [35] Desimoni E and Brunetti B 2015 *Chemosensors* **3** 70
- [36] Lai Q, Zhu S, Luo X, Zou M and Huang S 2012 *AIP Adv.* **2** 032146